Histol Histopathol (2025) 40: 89-100

Histology and Histopathology
From Cell Biology to Tissue Engineering

ORIGINAL ARTICLE Open Access

PYCR1 expresses in cancer-associated fibroblasts and accelerates the progression of C6 glioblastoma

Mingkun Zhang, Baibin Bi, Guangcun Liu and Xiaoyong Fan

Department of Neurosurgery, the First Affiliated Hospital of Shandong First Medical University, Shandong Medicine and Health Key Laboratory of Neurosurgery, Jinan, PR China.

*The two authors contributed equally

Summary. Background. Cancer-associated fibroblasts (CAFs) play important roles in tumor microenvironments. Pyrroline-5-carboxylate reductase 1 (PYCR1) is a potential cancer therapy target. This study aimed to explore the expression of PYCR1 in glioma-associated CAFs and analyze the effects of PYCR1 expression in CAFs on the proliferation of C6 glioma.

Methods. A rat glioma model was induced by injecting C6 cells in the right caudate putamen via a microliter syringe. After 14 days, tumor tissues were collected, and the levels of COL1A1 and PYCR1 were measured by immunohistochemistry. The colocalization of fibroblast activation protein α (FAP) and PYCR1 in tissues was measured by double-immunofluorescence. The CAFs were labeled by FAP and isolated from the tumor tissues using a fluorescence-activated cell sorting (FACS) machine. The isolated CAFs were further separated into CAFs with different PYCR1 expressions using the FACS machine. CAFs with different PYCR1 expressions were respectively cocultured with C6 cells or MUVECs for 48h using a Transwell permeable support. The invasion and proliferation of C6 cells were measured using a Transwell assay and colony formation assay, and the angiogenesis of MUVECs was measured using a Tube formation assay. The expression of COL1A1 and PYCR1 proteins in C6 cells and VEGF-A and EGF proteins in MUVECs was measured by western blotting. PYCR1 silencing in C6 cells was induced by PYCR1 siRNA transfection, the effects of which on the proliferation of C6 cells were measured using a wound healing assay, a Transwell assay, and western blotting.

Results. The PYCR1 and COL1A1 upregulation co-occurred in the rat glioma, and PYCR1 was expressed in CAFs. The CAF coculture enhanced the invasion and proliferation of C6 cells and the angiogenesis of MUVECs. Meanwhile, the levels of COL1A1 protein in C6 cells, and the levels of VEGF-A and EGF proteins in MUVECs were increased after CAF coculture. Moreover, the effects of CAF coculture were increased with PYCR1 expression in the CAF. Silencing PYCR1 suppressed the migration and invasion of C6 cells, and decreased the levels of COL1A1 and VEGF-A proteins in C6 cells.

Conclusions. PYCR1 is expressed in glioma-associated CAFs, and promotes the proliferation of C6 cells and angiogenesis of MUVECs, suggesting that targeting PYCR1 may be a therapeutic strategy for glioma.

Key words: Tumor microenvironment, Cancer-associated fibroblasts, MUVECs, COL1A1, Angiogenesis

Introduction

Cancer-associated fibroblasts (CAFs), an essential component of the tumor microenvironment (TME), are mesenchymal cells in the stroma of solid tumors and can promote tumor growth, extracellular matrix (ECM) remodeling, and chemoresistance (Mao et al., 2021). Several proteins have been used to identify CAFs, such as fibroblast activation protein α (FAP), fibroblast specific protein 1 (FSP1), and platelet-derived growth factor receptors (PDGFRs) (Li et al., 2020; Nurmik et al., 2020). In glioblastoma (GBM), including human and mouse GBM models, researchers have found that FAP-positive and PDGFRβ-positive pericytes are the major CAF-like stromal cells (Li et al., 2020). However, the molecular mechanism of GBM-associated CAFs in tumor progression is still an open question.

Pyrroline-5-carboxylate reductase 1 (PYCR1), a mitochondrial enzyme, facilitates the last step in glutamine-to-proline conversion, which catalyzes the NAD(P)H-dependent conversion of pyrroline-5-carboxylate to proline (Christensen et al., 2017; Bogner et al., 2021). Many studies have demonstrated that PYCR1 participates in the initiation and progression of

Corresponding Author: Xiaoyong Fan, No. 16766, Jingshi Road, Jinan, Shandong Province, PR China. e-mail: fanxiaoyong2023@163.com
www.hh.um.es. DOI: 10.14670/HH-18-762

multiple tumors through regulation of the immunosuppressive microenvironment and proline biosynthesis pathway (Bogner et al., 2021; Kay et al., 2022; Zhang et al., 2023). In GBM, it was reported that oncogenic isocitrate dehydrogenase 1 (*IDH1*) mutations promote the maintenance of mitochondrial redox homeostasis via enhancing proline synthesis through PYCR1 (Hollinshead et al., 2018), suggesting that PYCR1 participates in the progression of GBM. Importantly, researchers found that PYCR1 is highly expressed in the stroma of breast cancer patients and CAFs. Reducing PYCR1 levels in CAFs is sufficient to reduce tumor collagen production, tumor growth, and metastatic spread (Kay et al., 2022). Therefore, PYCR1 may have functions in the production of tumor ECM in the progression of GBM.

Collagen is the most abundant component of the tumor ECM (Kay et al., 2022). Collagen I (COL1A1) overexpression can enhance tumor formation and progression in the glioma model, and inhibition of COL1A1 prolongs animal survival by reducing the expression of mesenchymal-associated genes (Comba et al., 2022). Moreover, COL1A1 and fibronectin can collaborate to regulate glioma cell stemness via integrin αvβ3 and promote tumor growth (Zhong et al., 2021). However, the effects of PYCR1 on COL1A1 production in the glioma are unclear. Additionally, CAFs are the main contributors to tumor ECM stiffness and degradation (Najafi et al., 2019). CAFs interact with almost all cells within the TME, and a deeper understanding of PYCR1 in CAFs is needed for GBM therapy.

In this study, we used a rat glioma model to analyze the expression of PYCR1 in CAFs. Glioma-associated CAFs were isolated and separated into CAFs with different PYCR1 expressions. The separated CAFs were cocultured with C6 cells or mouse umbilical vein endothelial cells (MUVECs) to analyze the effects of PYCR1 expression in CAF on tumor progression. Moreover, silencing PYCR1 was used to confirm the effects of PYCR1 on C6 cells.

Materials and methods

Cell culture

C6 rat glioma cells (#C262) and MUVECs (#C1496) were purchased from Shanghai Enzyme-linked Biotechnology Co., Ltd (Shanghai, China). The C6 cells were cultured in F12K complete medium containing 10% fetal bovine serum (FBS), and the MUVECs were cultured in RPMI-1640 medium containing 10% FBS at 37°C and 5% CO_2. At about 80% confluency, cells were used for experiments.

Animal glioma model

Twelve male Sprague-Dawley rats (200-250 g) were housed with free access to food and water in an environment with 20-22°C, 45-55% humidity, and 12h/12h light/dark cycles.

According to the reported methods (Tian et al., 2022), six rats were anesthetized with 45 mg/kg pentobarbital sodium, and C6 cells (1×10^7 cells) were injected into the right caudate putamen (2.5 mm lateral, 1 mm anterior to the bregma, and 4 mm below the dura) via a microliter syringe over 5 min. After 14 days, the model rats were sacrificed through cervical dislocation. Tumor tissues were collected and stored at -80°C.

Immunohistochemistry

The tissues were fixed with 4% paraformaldehyde for 48h, dehydrated with gradient ethanol (80%, 90%, 95%, and 100%, 120 min each time), embedded in paraffin, and sectioned into slices (3 μm-thick). The slices were dewaxed with xylene three times, 15 min each time, and hydrated with gradient ethanol three times (100%, 95%, 90%, 80%, and 70%, 5 min each time). After washing with phosphate buffer saline (PBS), the slices were submerged in 3% H_2O_2 for 10 min and sodium citrate antigen repair solution (pH 6.0) for 30 min. After washing, the slices were blocked with 10% animal serum, then respectively incubated with rabbit COL1A1 antibody (#39952, 1:1000, Cell Signaling Technology) and rabbit PYCR1 antibody (#ab102601, 1:200, Abcam) at 4°C overnight. After washing, the slices were incubated with the goat anti-rabbit IgG H&L (#ab6721, 1:1000, Abcam) for 120 min at 37°C, and stained with diaminobenzidine. After washing, the slices were dehydrated with ethanol, cleared with xylene, and sealed with neutral gum. The results were observed under a light microscope (CKX53, Olympus, Japan).

Immunofluorescence

The slices (3 μm-thick) were dewaxed with xylene, hydrated with gradient ethanol, and blocked with BS-T containing 1% BSA (TBS). After washing, the slices were respectively incubated with FAP antibody (#66562, 1:200, Cell Signaling Technology) and PYCR1 antibody (#ab102601, 1:200, Abcam) overnight at 4°C. After washing with TBS, the slices were respectively incubated with Cy3-conjugated goat anti-rabbit IgG (H+L) antibody (#ab6939, 1:2000, Abcam) and FITC-conjugated goat anti-rabbit IgG (H+L) antibody (#ab6717, 1:2000, Abcam) for 90 min. After washing, the slices were stained with 4′,6-diamidino-2-phenylindole (DAPI) for 60s. After washing, dehydrating, clearing, and sealing, the slices were observed under a confocal microscope (#LSM800, Zeiss, Germany).

FAP-positive CAFs (FAP^+CAFs) isolation and culture

According to previous methods (Li et al., 2020), the rat tumors were excised, dissected, and cut into 1 mm fragments in DMEM, and transfected to a conical tube.

Then, the tissues were digested with accutase and DNase I (10 U/ml) at 37°C for 10 min at 200×g. After trituration, the tissues were passed through a 40 μm cell strainer to yield a single-cell suspension. After centrifugation (500×g, 10 min), CAFs were marked with a fibroblast-specific marker, FAP, and isolated using a fluorescence-activated cell sorting (FACS) machine (BD FACSDiscover™S8, USA). FAP-positive CAFs (FAP^+CAFs) were cultured in DMEM supplemented with 10% FBS, penicillin/streptomycin (100 U/100 μg), 2 mM L-glutamine and 1 mM sodium pyruvate at 37°C with 5% CO_2 (Kim et al., 2022). On reaching 70% confluence, the cells were used for experiments.

Separation of FAP^+CAFs with different PYCR1 expressions

FAP^+CAFs (1×10^6 cells) were washed with FACS buffer and blocked in FcR blocker for 20 min at 4°C, then incubated with Coralite®Plus 488-conjugated PYCR1 antibody (0.4 μg, #CL488-66510, Proteintech®) for 60 min at 4°C without light. After washing, the cells were incubated with anti-Rabbit IgG H&L (0.08 μg, #ab130805, Abcam) for 40 min at 4°C without light. The washed cells were transferred to FACS tubes and isolated using a FACS machine. The separated cells were cultured in DMEM supplemented with 10% FBS, penicillin/streptomycin (100 U/100 μg), 2 mM L-glutamine, and 1 mM sodium pyruvate at 37°C with 5% CO_2. The separated FAP+CAFs were confirmed by flow cytometry.

Flow cytometry

The FAP^+CAFs were separated by trypsin and placed into a conical centrifuge tube with a Pipetman® to dissociate any clumps. The cells were centrifuged and resuspended in an appropriate volume of Flow Cytometry Staining Buffer (#00-4222, Invitrogen) so that the final cell concentration is 1×10^7 cells/mL. In each tube, 50 μL of cells were added and then incubated with FAP antibody (1:100, #AAF01790, Aviva Systems Bio) and Coralite®Plus 488-conjugated PYCR1 antibody (0.4 μg, #CL488-66510, Proteintech®) for 40 min at 4°C with light. After washing with the Flow Cytometry Staining Buffer, the cells were centrifuged at 25°C twice (600×g, 5 min). After culturing for 60 min at 4°C, the cells were washed with staining buffer and centrifuged at 25°C twice (600×g, 5 min). Then, the cells were incubated with APC-anti-Rabbit IgG H&L (0.08 μg, #ab130805, Abcam) for 30 min at 4°C without light. After washing, the cells were centrifuged at 25°C twice and suspended in staining buffer. The results were obtained using flow cytometry (BD, FACSCanto II, USA).

FAP^+CAFs with different PYCR1 expressions were cocultured with C6 cells or MUVECs

Cells were cocultured with FAP+CAFs with different PYCR1 expressions for 48 h using a Transwell permeable support with a 0.4 μm polycarbonate membrane (Corning, Shanghai, China). According to previously reported methods (Cheng et al., 2017), FAP+CAFs with different PYCR1 (5×10^4 cells/well) were grown in a 6-well plate, and C6 cells (1×10^4 cells/well) or MUVECs (4×10^4 cells/well) were seeded in the upper chamber of a Transwell insert. The Transwell chambers were then inserted into the cell culture plate for 48h. Non-cocultured C6 cells or MUVECs were used as a control.

Cell transfection

The C6 cells (2×10^5/mL) were transfected with 1 μM PYRC1 small interfering RNA (siRNA) or control siRNA using Lipofectamine 2000 transfection reagent (Invitrogen) for 48h. The sequence of PYRC1 siRNA was 5'-CCGACATTGAGGACAGACA-3'. The results of siRNA were measured by western blotting.

Transwell assay

The invasion of C6 cells was measured using a Transwell assay. The pre-cooled Matrigel gel was diluted using a serum-free cell culture medium at 4°C. Matrigel gel (100 μL) was daubed on the surface of polyethylene terephthalate in the cell culture insert, then the insert was placed in a 24-well plate at 37°C for 3h. The cells (1×10^5/mL, 100 μL) were cultured in the upper chamber, and about 600 μL cell culture medium with 10% FBS were added to the lower chamber. After 24h, the chamber was fixed with 70% methanol solution for 60 min and stained with 1% crystal violet staining (#G1062, Solarbio, China) for 15 min. After washing with PBS three times, the cells were dried at room temperature. The numbers of cells were analyzed using ImageJ software.

Plate colony formation assay

The proliferation of C6 cells was measured using a plate colony formation assay. The C6 cells (1×10^3 cells/well) were cultured in an F12K complete medium containing 10% FBS for 10 days. The cells were fixed with 4% paraformaldehyde (#P1110, Solarbio, China) for 40 min, and stained with 1% crystal violet for 15 min. After washing, the cells were dried at room temperature and observed.

Tube formation assay

The angiogenesis of MUVECs was measured using the tube formation assay. MUVECs were digested with pancreatin and resuspended in culture medium, then 3×10^4 cells/well were cultured in a 96-well precoated with Matrigel for 24h. The tube formation of MUVEC was assessed by the number of branch points using ImageJ software.

Wound healing assay

The migration of C6 cells was measured using the wound healing assay. C6 cells (1×10^5/mL) were cultured in a six-well plate for 24h at 37°C with 5% CO_2. A gun head was used to make a scratch wound on the cells. The cells were washed with PBS three times, and cultured in the serum-free medium. The results were observed at 0h and 24h using a light microscope. Wound healing rate (%) = (Initial scratch area - scratch area at time t)/initial scratch area.

Western blotting

According to the reported procedures (Kurien and Scofield, 2006), levels of protein were measured using western blotting. C6 cells and MUVECs were respectively lysed with radioimmunoprecipitation assay (RIPA) lysis buffer (#P1038, Beyotime, China) and centrifuged (800×g, 4°C) for 20 min to obtain the total proteins. The protein concentration was detected using a BCA protein kit (#P0009, Beyotime, China). The total proteins and protein loading buffer (4:1) were mixed at 25°C and heated to 100°C for 5 min. Proteins (20 μg) were separated using a mPAGE® small gel electrophoresis system (Sigma-Aldrich) and transferred to immobilon®-P membranes (#IPV85R, Sigma-Aldrich). The membranes were blocked in 5% milk for 60 min and incubated with primary antibodies overnight at 4°C. The antibodies included COLA1 antibody (#39952, 1:1000, Cell Signaling Technology), PYCR1 antibody (#ab102601, 1:1000, Abcam), vascular endothelial growth factor A (VEGF-A) antibody (#50661, 1:1000, Cell Signaling Technology), epidermal growth factor (EGF) antibody (#ab184265, 1:1000, Abcam), and β-actin antibody (#4967, 1:1000, Cell Signaling Technology). After washing with TBS-0.01% Tween 20, membranes were incubated with goat anti-rabbit IgG H&L (#ab6721, 1:1000, Abcam) for 2h at 37°C. Proteins were visualized by exposing the membrane to an autoradiography film. The gray value of bands was analyzed using ImageJ software.

Statistics

Data were analyzed and plotted with GraphPad Prism software (v. 8.0, GraphPad Software Inc., La Jolla, CA, US). Data normality distribution was carried out by

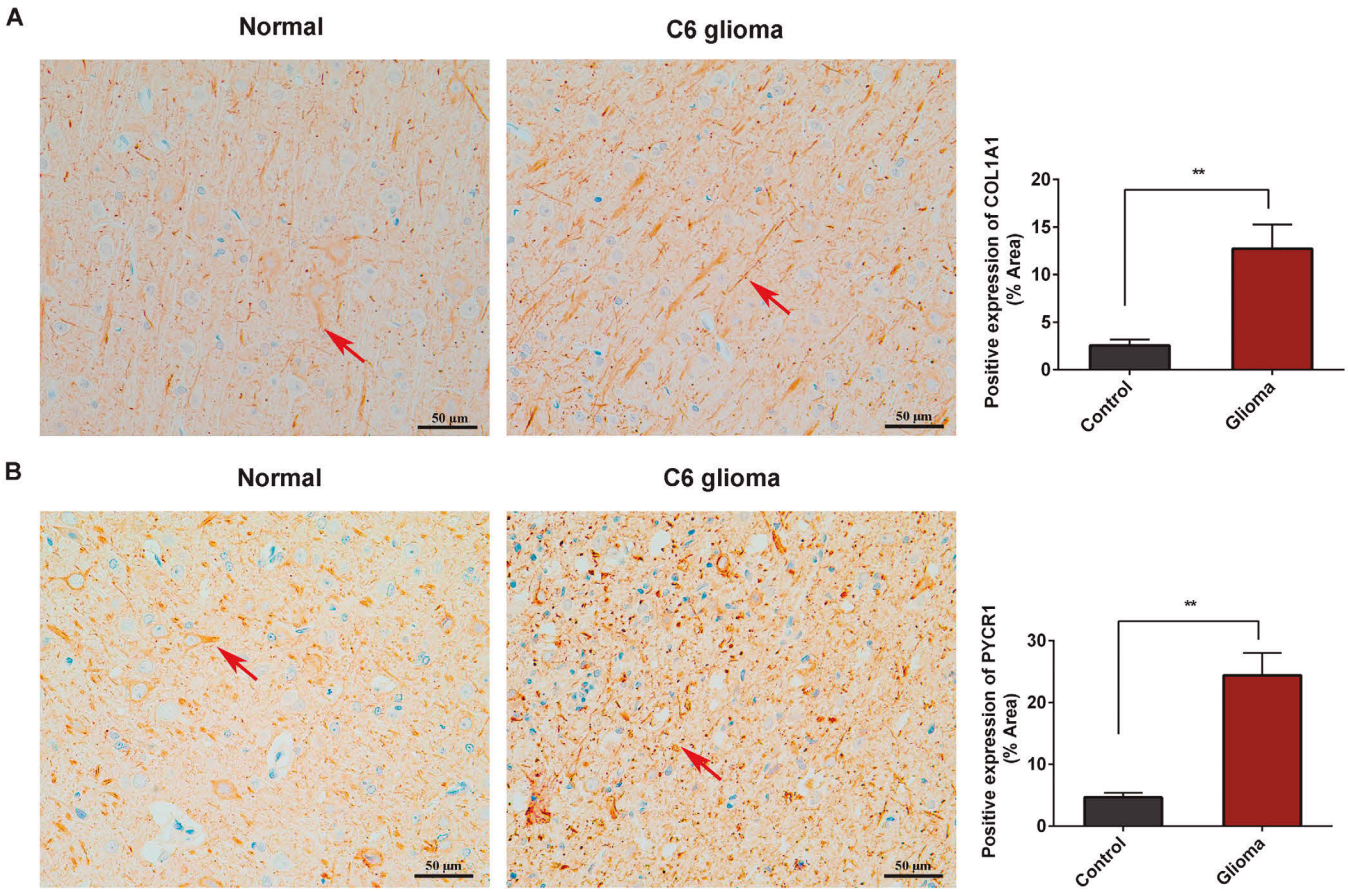

Fig. 1. Expression of COL1A1 and PYCR1 in the normal tissues and C6 glioma. The expression of COL1A1 **(A)** and PYCR1 **(B)** was measured via immunohistochemistry, scale = 50 μm. Positive expression (red arrows) of COL1A1 and PYCR1 was analyzed using ImageJ software. **p<0.01.

the Shapiro-Wilk test. The results were shown as mean ± standard deviation. A t-test was performed to assess significance between groups, and a one-way analysis of variance following the LSD test was performed to assess significance among groups. Statistical significance was designated as $p<0.05$.

Results

COL1A1 and PYCR1 upregulation occurred in the glioma

In the rat glioma, the expressions of COL1A1 (Fig. 1A) and PYCR1 (Fig. 1B) were significantly higher than those in control tissues ($p<0.01$). The colocalization of FAP (red) and PYCR1 (green) in tissues was observed using double-immunofluorescence (Fig. 2A). No co-expression was observed in control tissues, but about 70% of double-labeling cells were observed in the glioma (Fig. 2B, $p<0.01$). These preliminary data showed that CAFs produced PYCR1 and promoted COL1A1 expression in the glioma.

Separation of FAP$^+$CAFs with different PYCR1 expression

As shown in Figure 3A, FAP$^+$CAFs with different PYCR1 expression were successfully obtained. The FAP$^+$CAFs with low PYCR1 expression (≤10%) were named PYCR1^{low}/FAP$^+$CAFs, and FAP$^+$CAFs with high PYCR1 expression (≥60%) were named PYCR1^{high}/

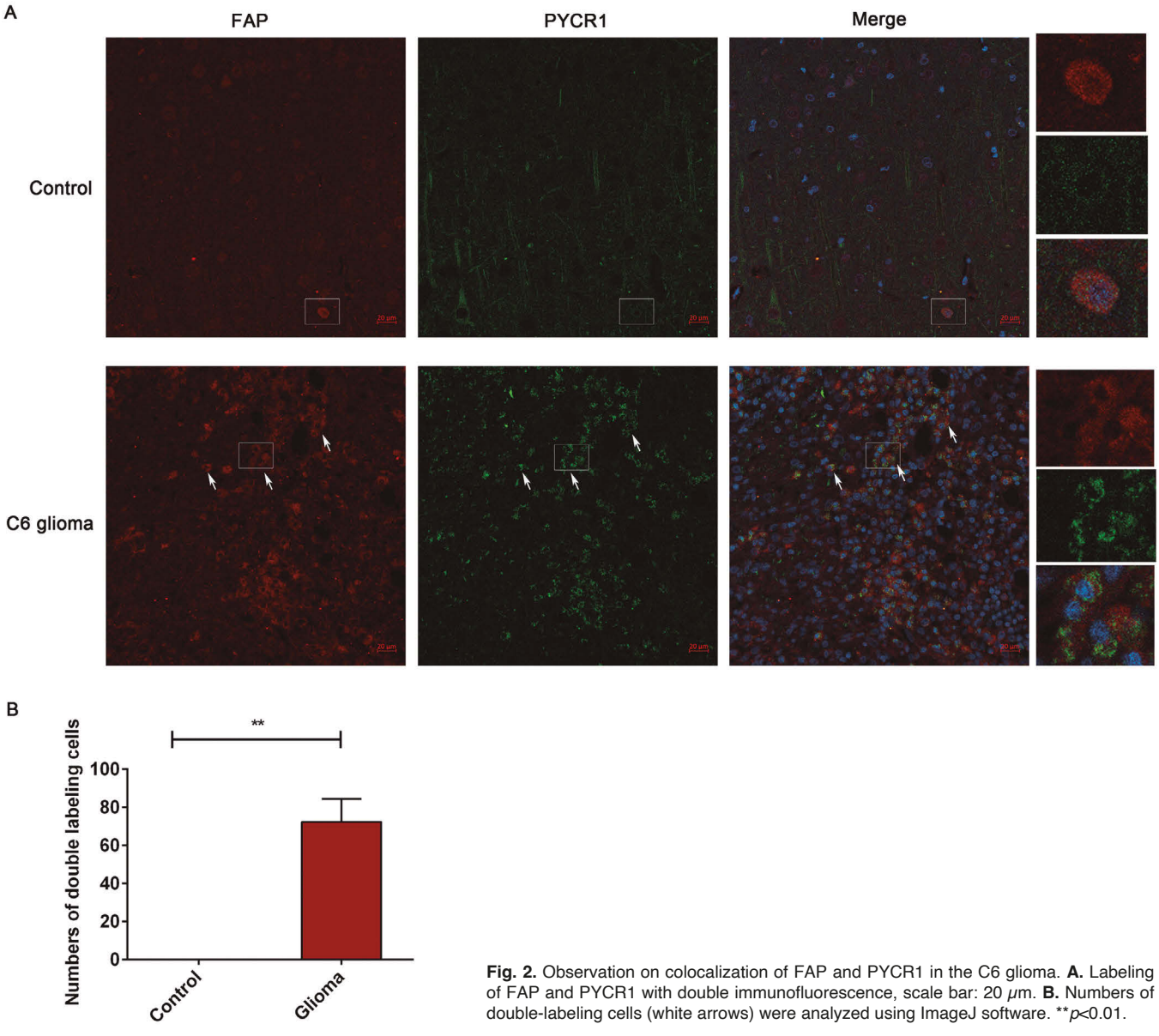

Fig. 2. Observation on colocalization of FAP and PYCR1 in the C6 glioma. **A.** Labeling of FAP and PYCR1 with double immunofluorescence, scale bar: 20 μm. **B.** Numbers of double-labeling cells (white arrows) were analyzed using ImageJ software. $^{**}p<0.01$.

FAP$^+$CAFs. Unseparated FAP$^+$CAFs were used as the control, where PYCR1 expression was about 20-40%. To confirm the levels of PYCR1 protein in separated FAP$^+$CAFs, the level of PYCR1 protein was observed at 0h, 24h, and 48h after separation (Fig. 3B). Over time, the level of PYCR1 protein was not changed in the separated FAP$^+$CAFs. To analyze the effects of FAP$^+$CAFs with different PYCR1 expression on C6 cells or MUVECs, FAP$^+$CAFs were cocultured with C6 cells or MUVECs for 48h (Fig. 3C).

PYCR1 in FAP$^+$CAFs enhanced the invasion and proliferation of C6 cells

Through observing the invasion of C6 cells using a Transwell assay (Fig. 4A), FAP$^+$CAFs coculture significantly enhanced the invasion of C6 cells (p<0.05). Moreover, the invasion of C6 cells was increased with PYCR1 expression in FAP$^+$CAFs (p<0.05). Through observing the proliferation of C6 cells using the colony assay (Fig. 4B), the proliferation of C6 cells was significantly increased after FAP$^+$CAFs coculture (p<0.05), and cell proliferation was increased with PYCR1 expression in FAP$^+$CAFs (p<0.05). The levels of PYCR1 and COL1A1 proteins in C6 cells were observed by western blotting (Fig. 5A), and their levels were clearly upregulated after coculture with FAP$^+$CAFs (p<0.05). Moreover, the levels of these proteins were increased with PYCR1 expression in FAP$^+$CAFs (p<0.05).

PYCR1 in FAP+CAFs enhanced the angiogenesis of MUVECs

Through observing the angiogenesis of MUVECs using the tube formation assay (Fig. 6A), FAP$^+$CAFs coculture significantly enhanced the angiogenesis of MUVECs (p<0.05). Moreover, the angiogenesis of

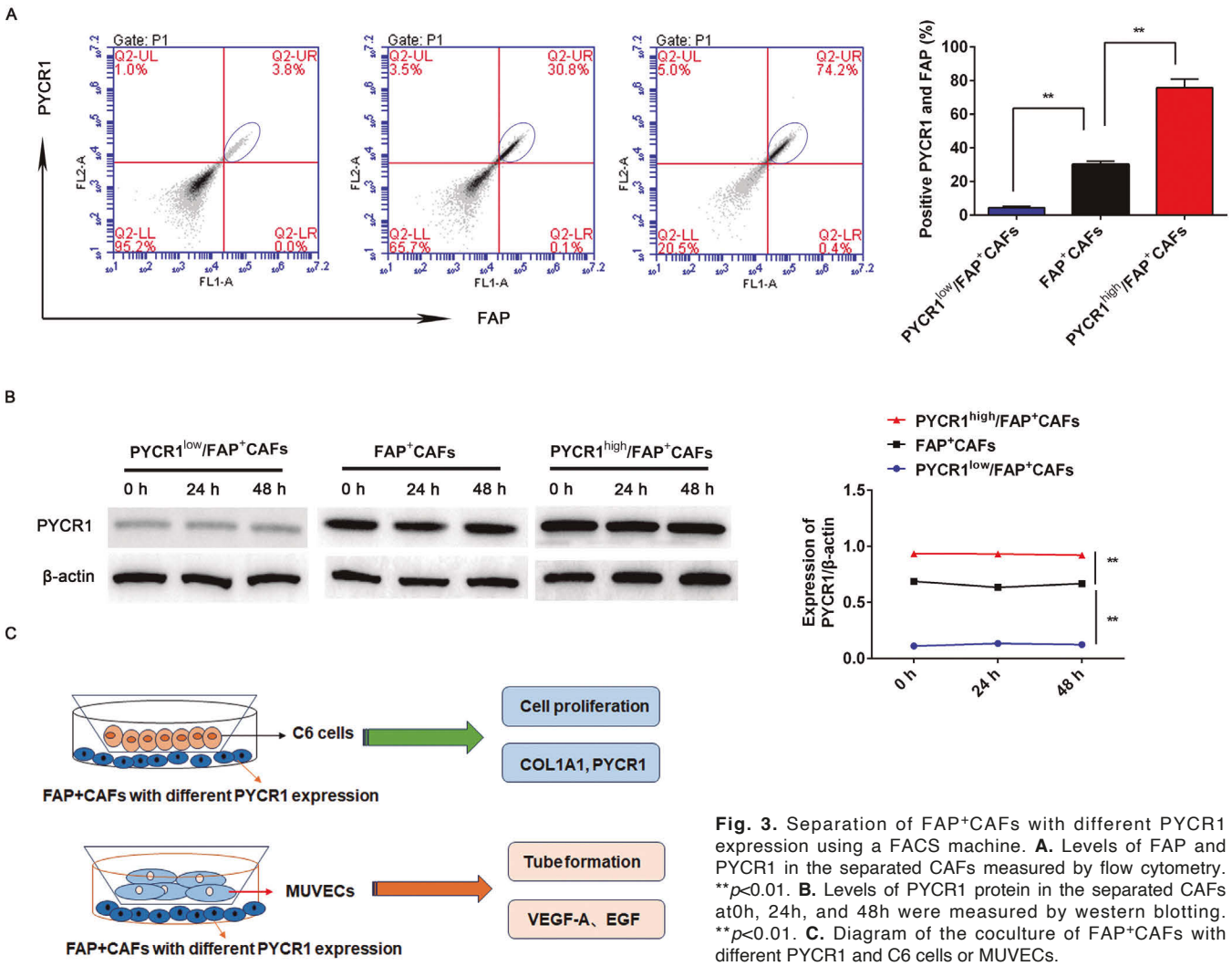

Fig. 3. Separation of FAP$^+$CAFs with different PYCR1 expression using a FACS machine. **A.** Levels of FAP and PYCR1 in the separated CAFs measured by flow cytometry. **p<0.01. **B.** Levels of PYCR1 protein in the separated CAFs at0h, 24h, and 48h were measured by western blotting. **p<0.01. **C.** Diagram of the coculture of FAP$^+$CAFs with different PYCR1 and C6 cells or MUVECs.

MUVECs was increased with PYCR1 expression in FAP^{+}CAFs (p<0.05). The levels of VEGF-A and EGF proteins in MUVECs were observed (Fig. 5B), and the levels of these proteins were clearly upregulated after coculture with FAP^{+}CAFs (p<0.05). Meanwhile, the levels of the two proteins were increased with PYCR1 expression in FAP^{+}CAFs (p<0.05).

PYCR1 silencing inhibited the migration and invasion of C6 cells

To further confirm the roles of PYCR1 in C6 cells, PYCR1 silencing in C6 cells was established by PYCR1 siRNA transfection. The results of western blotting confirmed the PYCR1 silencing in C6 cells (Fig. 7A). By observing the migration of C6 cells using a wound healing assay (Fig. 7B), PYCR1 silencing significantly suppressed the migration of C6 cells (p<0.01). By observing the invasion of C6 cells using the Transwell assay (Fig. 8A), PYCR1 silencing significantly suppressed the invasion of C6 cells (p<0.01). Moreover, the levels of COL1A1 and VEGF-A proteins in C6 cells were clearly downregulated by PYCR1 siRNA transfection (p<0.01).

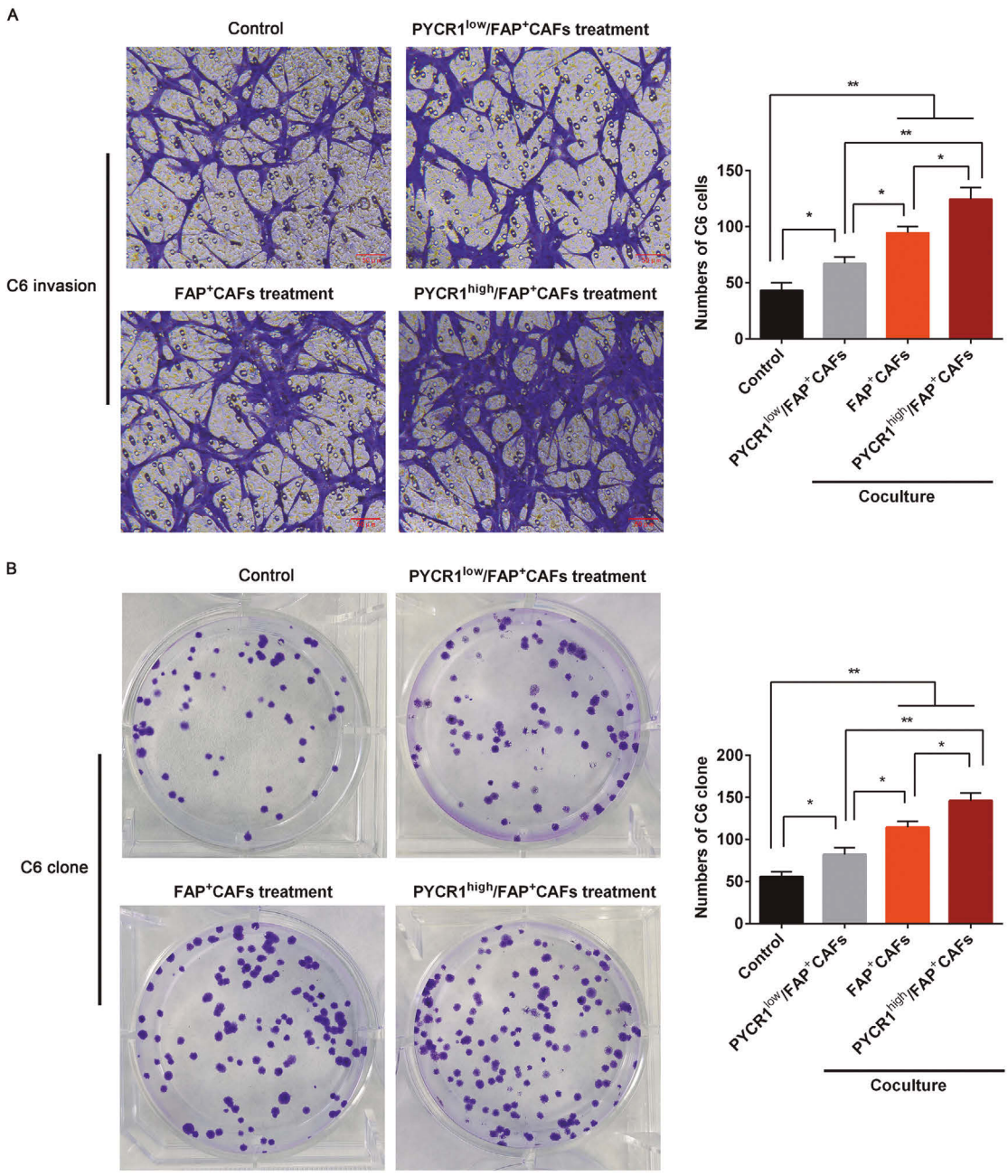

Fig. 4. Effects of FAP^{+}CAFs with different PYCR1 expression on invasion and proliferation of C6 cells. **A.** The invasion of C6 cells was measured by a Transwell assay. **B.** The proliferation of C6 cells was measured using a plate colony formation assay. *p<0.05, **p<0.01.

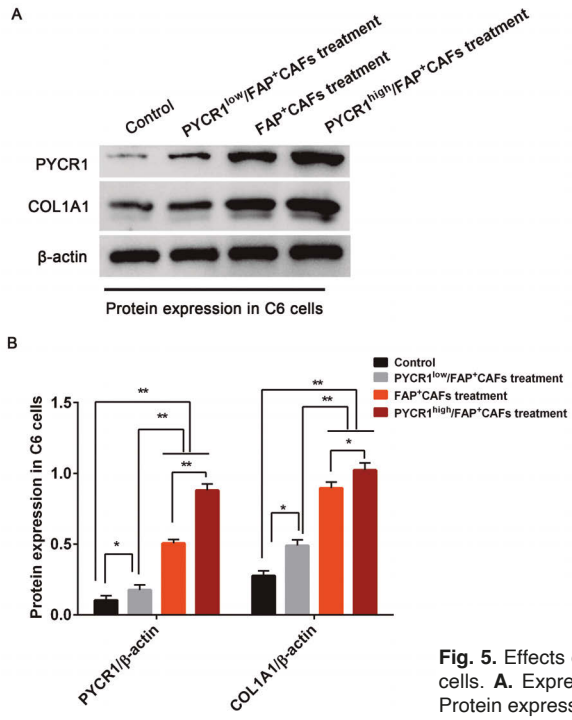

Discussion

Glioma is the most common brain tumor with a poor prognosis in the central nervous system, and C6 rat glioblastoma cells provide scientists with the possibility to study brain cancer (Hacioglu et al., 2021; Kar et al., 2021, 2023). Many cell mechanisms have been found in glioma using the C6 cells, such as the ferroptosis (Kar et al., 2023), oxidative and inflammation signaling pathways (Hacioglu et al., 2021), and thiol/disulfide balance destruction (Kar et al., 2021). However, the molecular mechanisms of CAFs in gliomas are little studied. In this study, the results showed that PYCR1 is expressed in glioma-associated FAP$^+$CAFs and related to COL1A1 production. Moreover, FAP$^+$CAFs coculture enhanced the proliferation of C6 cells and angiogenesis of MUVECs, and the effects of coculture were increased with PYCR1 expression in FAP$^+$CAFs (Fig. 9). PYCR1 silencing suppressed the migration and invasion of C6

Fig. 5. Effects of FAP$^+$CAFs with different PYCR1 expressions on COL1A1 protein levels in C6 cells. **A.** Expression of PYCR1 and COL1A1 proteins was measured by western blotting. **B.** Protein expression was analyzed using ImageJ software. *p<0.05, **p<0.01.

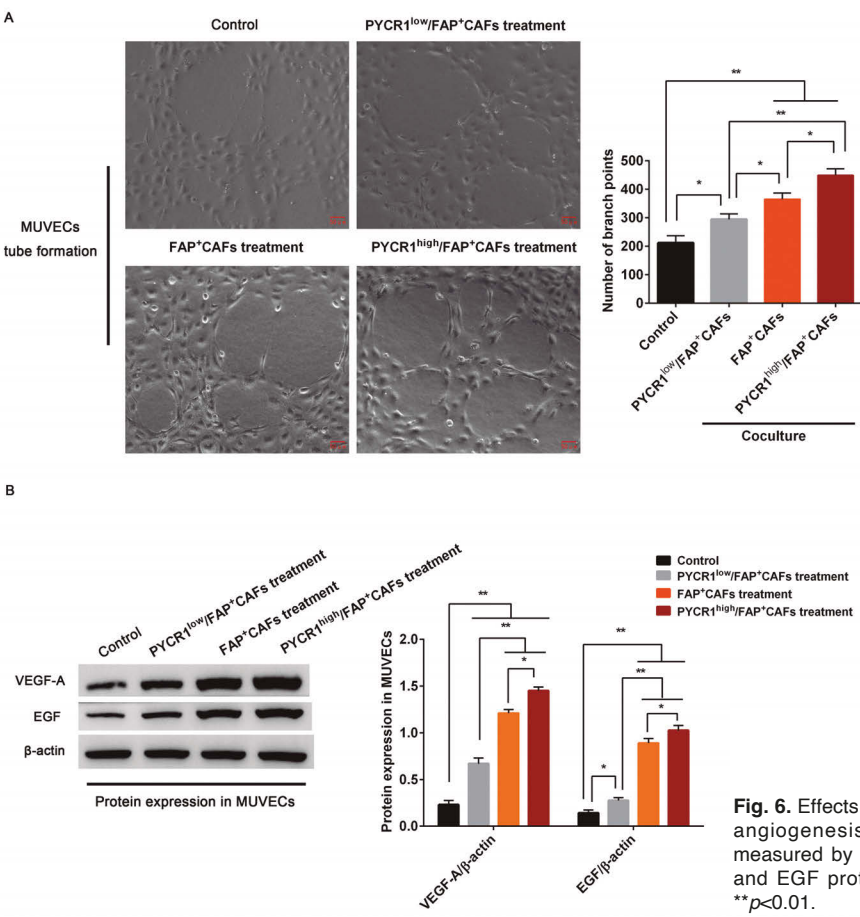

Fig. 6. Effects of FAP$^+$CAFs with different PYCR1 expression on the angiogenesis of MUVECs. **A.** Angiogenesis of MUVECs was measured by the tube formation assay. **B.** Expression of VEGF-A and EGF proteins was measured by western blotting. *p< 0.05, **p<0.01.

cells. These results indicate that targeting PYCR1 is a therapeutic strategy for GBM.

In glioma, CAFs can secrete growth factors, inflammatory ligands, and ECM proteins to regulate the TME (Trylcova et al., 2015; Li et al., 2020; Biffi and Tuveson, 2021). The production of abundant collagen-rich ECM is a trait that CAFs acquire during the transition from normal to activated fibroblasts (Kay et al., 2022). Moreover, PYCR1 provides proline for collagen biosynthesis in breast cancer-associated CAFs (Kay et al., 2022). FAP is widely considered one of the most reliable CAF-makers and is positively expressed in glioma-associated CAFs (Li et al., 2020). Consistent with these findings, our study revealed that COL1A1, the most abundant collagen, and PYCR1 are highly expressed in the rat glioma. Moreover, FAP and PYCR1 colocalized in the rat glioma, suggesting that PYCR1 regulates CAF activation and tumor progression.

As a mitochondrial NADH-oxidizing enzyme, PYCR1 activity is enhanced to increase the synthesis of proline in mutant *IDH1* glioma cells (Hollinshead et al., 2018). To further confirm the effects of PYCR1 in CAFs on tumor progression, FAP^{+}CAFs with different PYCR1 were cocultured with C6 cells or MUVECs using a Transwell permeable support, and the results showed the invasion and proliferation of C6 cells; the angiogenesis of MUVECs were significantly enhanced after FAP^{+}CAFs coculture. Moreover, the effects were increased with increased PYCR1 in FAP^{+}CAFs. Additionally, the levels of the COL1A1 protein in C6

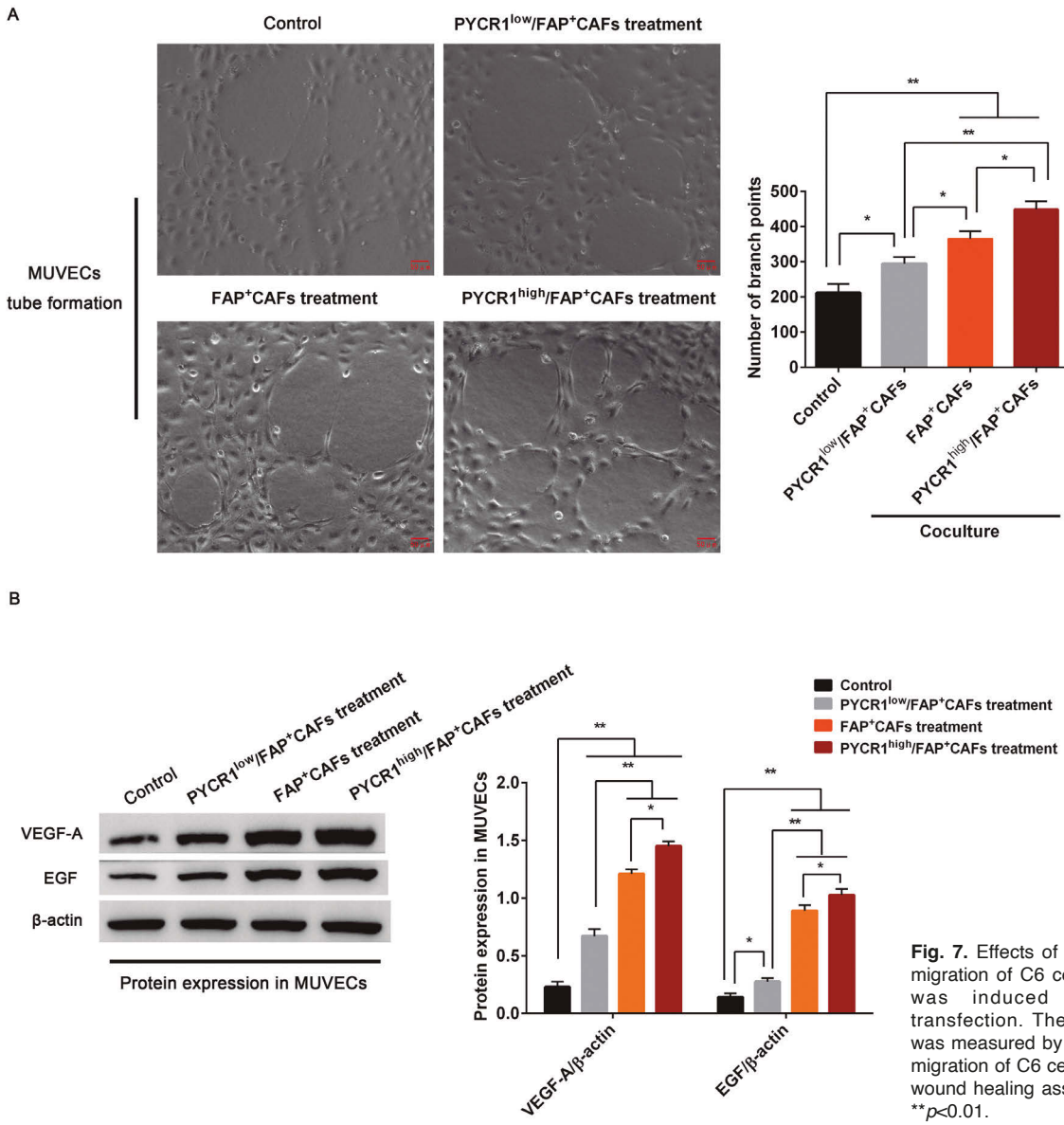

Fig. 7. Effects of PYCR1 silencing on the migration of C6 cells. A. PYCR1 silencing was induced by PYCR1 siRNA transfection. The expression of PYCR1 was measured by western blotting. **B.** The migration of C6 cells was measured by the wound healing assay. NS: no significance. $^{**}p<0.01$.

cells and the levels of VEGF-A and EGF proteins in MUVECs were increased after FAP^{+}CAFs coculture, and the increased proteins were increased with PYCR1 expression in FAP^{+}CAFs. The COL1A1 overexpression enhances tumor formation and progression in glioma (Comba et al., 2022; Ren et al., 2022). As an angiogenic inducer, EGF signaling positively regulates VEGF production in many cancers, including human GBM (Nicolas et al., 2019). The EGF receptor is activated by EGF, and further leads to the secretion of VEGF in GBM (Nicolas et al., 2019). Additionally, the EGF signal can regulate the mitogen-activated protein kinase/extracellular signal-regulated kinase (MAPK/ERK) pathway and the phosphatidylinositol 3-kinase (PI3K) pathway to

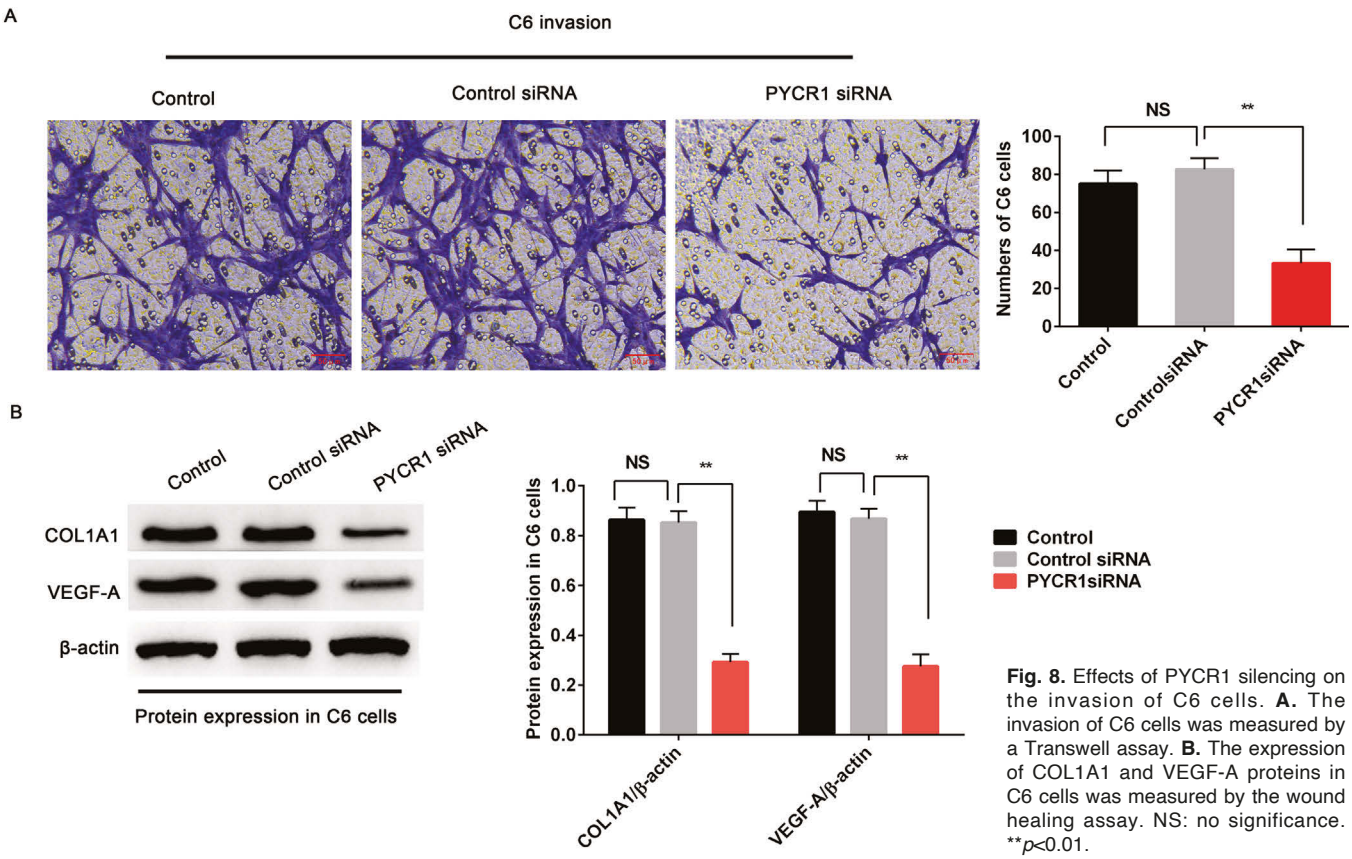

Fig. 8. Effects of PYCR1 silencing on the invasion of C6 cells. **A.** The invasion of C6 cells was measured by a Transwell assay. **B.** The expression of COL1A1 and VEGF-A proteins in C6 cells was measured by the wound healing assay. NS: no significance. $^{**}p<0.01$.

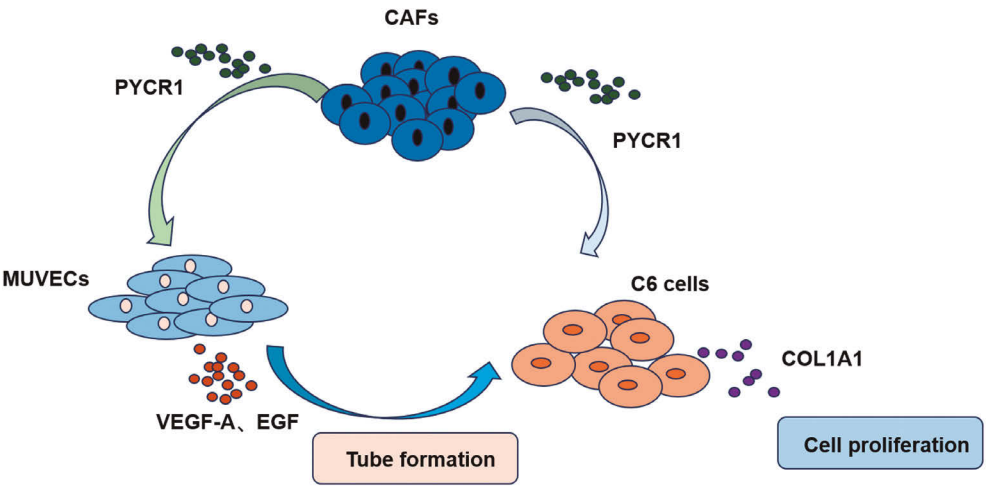

Fig. 9. Diagram of PYCR1 produced by CAFs on the progression of C6 glioma. PYCR1 produced by CAFs promotes tumor growth by increasing the expressions of COL1A1, VEGF-A, and EGF proteins in cancer cells and MUVECs.

regulate angiogenesis in GBM (Wu et al., 2000; Steinbach et al., 2004; Nicolas et al., 2019). Based on these studies, our study demonstrates that PYCR1 produced by CAFs accelerates the progression of GBM, and targeting PYCR1 is a therapeutic strategy for GBM.

This study also confirmed that reducing PYCR1 suppressed the migration and invasion of C6 cells. However, the impact of PYCR1 expression in CAFs on treatment response in glioma requires further study. Effectively targeting CAF metabolism in GBM is still an open question, since metabolic vulnerabilities of CAFs and cancer cells can be different, and crosstalk between the cell types creates an intertwined metabolic network. Further experiments are needed to assess other metabolites that contribute to CAF metabolism in GBM to understand CAF metabolic reprogramming.

Conclusions

Our study revealed that PYCR1 and COL1A1 upregulation co-occurred in C6 rat GBM, and PYCR1 was expressed in GBM-associated CAFs. CAF coculture enhanced the proliferation of C6 cells and angiogenesis of MUVECs, and the effects were increased with PYCR1 expression in CAFs. Our study implies that targeting PYCR1 may offer an opportunity to attack GBM.

Acknowledgements. The manuscript was edited by Charlesworth Author Services.

Ethical Approval. All experimental procedures were performed in accordance with the guidelines of Animal Care and Use of the First Affiliated Hospital of Shandong First Medical University (No. 20130155), and the ARRIVE guidelines for the reporting of animal experiments.

Consent for Publication. Not applicable.

Availability of Data and Material. All data in this study are available from the corresponding author upon request.

Competing Interests. The authors declare that they have no competing interests.

Funding. Not applicable.

Authors' Contributions. M.Z. and B.B. participated in the study design, experimental work, and data collection. M.Z. prepared the manuscript. B.B. and G.L. coordinated experimental work, data collection, and software application. X.F. partook in the study design and manuscript editing. All authors read and agreed with the final manuscript.

References

Biffi G. and Tuveson D.A. (2021). Diversity and biology of cancer-associated fibroblasts. Physiol. Rev. 101, 147-176.

Bogner A.N., Stiers K.M. and Tanner J.J. (2021). Structure, biochemistry, and gene expression patterns of the proline biosynthetic enzyme pyrroline-5-carboxylate reductase (PYCR), an emerging cancer therapy target. Amino Acids 53, 1817-1834.

Cheng H.W., Chen Y.F., Wong J.M., Weng C.W., Chen H.Y., Yu S.L., Chen H.W., Yuan A. and Chen J.J. (2017). Cancer cells increase endothelial cell tube formation and survival by activating the PI3K/Akt signalling pathway. J. Exp. Clin. Cancer. Res. 36, 27.

Christensen E.M., Patel S.M., Korasick D.A., Campbell A.C., Krause K.L., Becker D.F. and Tanner J.J. (2017). Resolving the cofactor-binding site in the proline biosynthetic enzyme human pyrroline-5-carboxylate reductase 1. J. Biol. Chem. 292, 7233-7243.

Comba A., Faisal S.M., Dunn P.J., Argento A.E., Hollon T.C., Al-Holou W.N., Varela M.L., Zamler D.B., Quass G.L., Apostolides P.F., Abel C., 2nd, Brown C.E., Kish P. E., Kahana A., Kleer C.G., Motsch S., Castro M.G. and Lowenstein P.R. (2022). Spatiotemporal analysis of glioma heterogeneity reveals COL1A1 as an actionable target to disrupt tumor progression. Nat. Commun. 13, 3606.

Hacioglu C., Kar F., Kacar S., Sahinturk V. and Kanbak G. (2021). Bexarotene inhibits cell proliferation by inducing oxidative stress, DNA damage and apoptosis via PPARγ/ NF-κB signaling pathway in C6 glioma cells. Med. Oncol. 38, 31.

Hollinshead K.E.R., Munford H., Eales K.L., Bardella C., Li C., Escribano-Gonzalez C., Thakker A., Nonnenmacher Y., Kluckova K., Jeeves M., Murren R., Cuozzo F., Ye D., Laurenti G., Zhu W., Hiller K., Hodson D.J., Hua W., Tomlinson I.P., Ludwig C., Mao Y. and Tennant D.A. (2018). Oncogenic IDH1 mutations promote enhanced proline synthesis through PYCR1 to support the maintenance of mitochondrial redox momeostasis. Cell. Rep. 22, 3107-3114.

Kar F., Hacioğlu C. and Kaçar S. (2023). The dual role of boron *in vitro* neurotoxication of glioblastoma cells via SEMA3F/NRP2 and ferroptosis signaling pathways. Environ. Toxicol. 38, 70-77.

Kar F., Kacar S., Hacioglu C., Kanbak G. and Sahinturk V. (2021). Concanavalin A induces apoptosis in a dose-dependent manner by modulating thiol/disulfide homeostasis in C6 glioblastoma cells. J. Biochem. Mol. Toxicol. 35, e22742.

Kay E.J., Paterson K., Riera-Domingo C., Sumpton D., Däbritz J.H.M., Tardito S., Boldrini C., Hernandez-Fernaud J.R., Athineos D., Dhayade S., Stepanova E., Gjerga E., Neilson L.J., Lilla S., Hedley A., Koulouras G., McGregor G., Jamieson C., Johnson R.M., Park M., Kirschner K., Miller C., Kamphorst J.J., Loayza-Puch F., Saez-Rodriguez J., Mazzone M., Blyth K., Zagnoni M. and Zanivan S. (2022). Cancer-associated fibroblasts require proline synthesis by PYCR1 for the deposition of pro-tumorigenic extracellular matrix. Nat. Metab. 4, 693-710.

Kim H.J., Yang K., Kim K., Lee Y.J., Lee S., Ahn S.Y., Ahn Y. H. and Kang J.L. (2022). Reprogramming of cancer-associated fibroblasts by apoptotic cancer cells inhibits lung metastasis via Notch1-WISP-1 signaling. Cell. Mol. Immunol. 19, 1373-1391.

Kurien B.T. and Scofield R.H. (2006). Western blotting. Methods 38, 283-293.

Li M., Li G., Kiyokawa J., Tirmizi Z., Richardson L.G., Ning J., Das S., Martuza R.L., Stemmer-Rachamimov A., Rabkin S.D. and Wakimoto H. (2020). Characterization and oncolytic virus targeting of FAP-expressing tumor-associated pericytes in glioblastoma. Acta Neuropathol. Commun. 8, 221.

Mao X., Xu J., Wang W., Liang C., Hua J., Liu J., Zhang B., Meng Q., Yu X. and Shi S. (2021). Crosstalk between cancer-associated fibroblasts and immune cells in the tumor microenvironment: new findings and future perspectives. Mol. Cancer 20, 131.

Najafi M., Farhood B. and Mortezaee K. (2019). Extracellular matrix (ECM) stiffness and degradation as cancer drivers. J. Cell. Biochem. 120, 2782-2790.

Nicolas S., Abdellatef S., Haddad M.A., Fakhoury I. and El-Sibai M. (2019). Hypoxia and EGF stimulation regulate VEGF expression in

human glioblastoma multiforme (GBM) Cells by differential regulation of the PI3K/Rho-GTPase and MAPK pathways. Cells 8, 1397.

Nurmik M., Ullmann P., Rodriguez F., Haan S. and Letellier E. (2020). In search of definitions: Cancer-associated fibroblasts and their markers. Int. J. Cancer 146, 895-905.

Ren J., Da J. and Hu N. (2022). Identification of COL1A1 associated with immune infiltration in brain lower grade glioma. PLoS. One 17, e0269533.

Steinbach J.P., Klumpp A., Wolburg H. and Weller M. (2004). Inhibition of epidermal growth factor receptor signaling protects human malignant glioma cells from hypoxia-induced cell death. Cancer Res. 64, 1575-1578.

Tian Z., Sun C. and Liu J. (2022). Pelargonidin inhibits vascularization and metastasis of brain gliomas by blocking the PI3K/AKT/mTOR pathway. J. Biosci. 47, 64.

Trylcova J., Busek P., Smetana K., Jr., Balaziova E., Dvorankova B., Mifkova A. and Sedo A. (2015). Effect of cancer-associated fibroblasts on the migration of glioma cells *in vitro*. Tumou. Biol. 36, 5873-5879.

Wu C.J., Chen Z., Ullrich A., Greene M.I. and O'Rourke D.M. (2000). Inhibition of EGFR-mediated phosphoinositide-3-OH kinase (PI3-K) signaling and glioblastoma phenotype by signal-regulatory proteins (SIRPs). Oncogene 19, 3999-4010.

Zhang L., Zhao X., Wang E., Yang Y., Hu L., Xu H. and Zhang B. (2023). PYCR1 promotes the malignant progression of lung cancer through the JAK-STAT3 signaling pathway via PRODH-dependent glutamine synthesize. Transl. Oncol. 32, 101667.

Zhong C., Tao B., Tang F., Yang X., Peng T., You J., Xia K., Xia X., Chen L. and Peng L. (2021). Remodeling cancer stemness by collagen/fibronectin via the AKT and CDC42 signaling pathway crosstalk in glioma. Theranostics 11, 1991-2005.

Accepted May 15, 2024